

Similarity laws of the fiber-matrix interface crack in Fiber-Reinforced Polymer Composites

Luca Di Stasio^{a,b}, Janis Varna^a, Zoubir Ayadi^b

^a*Luleå University of Technology, University Campus, SE-97187 Luleå, Sweden*

^b*Université de Lorraine, EEIGM, IJL, 6 Rue Bastien Lepage, F-54010 Nancy, France*

Abstract

Keywords: Fiber Reinforced Polymer Composite (FRPC), Debonding, Similarity, Dimensional analysis

1. Introduction

One of the most promising developments in Fiber Reinforced Polymer Composites (FRPCs) for advanced structural applications is currently represented by *thin-ply* laminates [1]. Constituted by extremely thin plies, with t_{90° as
5 small as just $\sim 4 - 5$ fiber diameters, this family of laminates is characterized by its damage tolerance, in particular the capability of delaying to higher strains and even suppressing the onset and propagation of transverse cracks [2]. The recent experimental assessment of transverse cracks suppression in *thin-ply* laminates [3, 4, 5] validates the existence of a *ply-thickness* effect [5] at scales
10 $10x$ smaller than those at which it was originally observed at the end of the 1970's [6].

Onset of transverse cracks coincides at the microscopic level with the formation of fiber/matrix interface cracks [7], or debonds. After the inter-fiber stress [8] and strain concentration [9] causes the matrix to fail at or close to the fiber in-
15 terface, debonds grow along the fiber arc direction until a maximum or critical size is reached. If the applied load is increased, debonds move into the matrix or

“kink” out of the fiber/matrix interface [10, 11]. Coalescence of debonds then occurs, which corresponds macroscopically to through-the-thickness transverse crack propagation [10, 12]. Finally, propagation through the specimen width
20 occurs [10].

Given that *thin-ply*s, as previously noted, can reach nowadays thicknesses of just $\sim 4 - 5$ fiber diameters, the characteristic size of the ply, i.e. the thickness t_{90° , is now comparable in magnitude to the characteristic size of debonds, i.e. the fiber diameter $2R_f$, such that $t_{90^\circ}/(2R_f) \sim \mathcal{O}(1)$. This has motivated
25 in recent years a renewed interest in debond growth modeling [13, 14, 15, 16]. Since the elastic solution to the interface crack problem implies an oscillating solution at the crack tip [17] in the *open* case (crack faces not in contact), Stress Intensify Factors (SIFs) are not defined and debond growth characterization has focused on the determination of Mode I, Mode II and total Energy Release Rate
30 (ERR). Many authors have reported their results in normalized form [11, 18, 19], by defining a reference ERR G_0 . The definition of such reference ERR would be useful to establish similarity laws and thus to allow comparisons between different material systems, scales, loads and microstructural arrangement. However, no agreement can be found in the literature on the very definition of G_0 and
35 expressions vary between authors. Furthermore, no clear derivation of G_0 has been proposed. In this brief contribution, we provide a derivation of G_0 based on arguments of dimensional analysis, material homogenization and fracture mechanics; we then apply the derived expression of reference ERR to the analysis of debond growth in Representative Volume Elements (RVEs) of UD composites
40 and cross-ply laminates.

2. Representative Volume Elements (RVEs) and Finite Element (FE) discretization

In this contribution, we analyze debond initiation and propagation in Representative Volume Elements (RVEs) of Uni-Directional (UD) composites and
45 $[0_{m \cdot k \cdot 2L}^\circ, 90_{k \cdot 2L}^\circ, 0_{m \cdot k \cdot 2L}^\circ]$ laminates. Given a global reference frame with axis x ,

y and z , both types of composites are modeled as plates lying in the $x-y$ plane, with the through-the-thickness direction thus aligned with the z axis. The UD composite 0° direction is parallel to the y axis, while the cross-ply 0° direction is parallel to the x axis. Both composites are loaded in tension along the x axis, which thus corresponds to: transverse loading of the UD specimen; axial loading of the cross-ply specimen. In both composites, damage is present only in the form of fiber/matrix interface cracks, or debonds. In cross-ply, debonds are assumed to be present only in the central 90° ply. Given that: first, in the presence of a load in the x -direction, in both lay-ups the y -strain due to Poisson's effect is very small; second, debond size is assumed to be considerably larger in the fiber than in the arc direction [10]; third, we are interested in studying debond growth along the arc direction; we can consider $2D$ models under plane strain conditions defined in the $x-z$ plane. Although generalized plane strain conditions would represent a more appropriate modeling choice, it would limit the ability to compare with previous results. Simple plane strain conditions are thus preferred. UD composites and 90° plies are characterized by a regular microstructure following a square-packing configuration of fibers, built through the repetition of a one-fiber unit cell along the horizontal and the vertical direction. This unit cell is a square with the center occupied by one fiber of radius $R_f = 1 \mu m$ and the rest of the element constituted by matrix. The size of the one-fiber unit cell is $2L \times 2L$, such that:


$$L = \frac{R_f}{2} \sqrt{\frac{\pi}{V_f}}, \quad (1)$$

where V_f is the fiber volume fraction, here assumed to be 60%. It is worth to specify at this point that the choice $R_f = 1 \mu m$ is arbitrary and stems from the fact that ERR, in the contest of a linear elastic solution as the one considered in this article, is proportional to the geometrical dimensions of the model. Simplicity is thus the main reason for this choice. Also, V_f is always the same in the one-fiber unit cell and the entire RVE, i.e. no fiber clustering is analyzed in this work. In the case of cross-ply laminates, the 0° layer is

homogenized with properties evaluated according to the Concentric Cylinders
 75 Assembly with Self-Consistent Shear (CCA-SCS) model [28, 29]. A glass fiber-
 epoxy system is considered for both UD and cross-ply laminates. Material
 properties are reported in Table 1.

Table 1: Summary of mechanical properties of fiber, matrix and UD layer.

Material	V_f [%]	E_L [GPa]	E_T [GPa]	G_{LT} [GPa]	ν_{LT} [-]	ν_{TT} [-]
Glass fiber	-	70.0	70.0	29.2	0.2	0.2
Epoxy	-	3.5	3.5	1.25	0.4	0.4
UD	60.0	43.442	13.714	4.315	0.273	0.465

The use of coupling conditions allows the study of a Repeating Unit Cells
 (RUC) of reduced size with respect to the corresponding RVE, which translates
 80 in a gain in terms of computational time and memory usage during the eval-
 uation of Finite Element (FE) solution. The RVEs studied in this article are
 reported in Figure ?? with the corresponding RUC highlighted by dashed line
 (in blue in the online color version) and with symmetry and coupling condi-
 tions represented by rollers () . Details about the central one-fiber unit cell are
 85 shown in Figure 1. Notice that the analysis, in terms of stresses and Energy
 Release Rate (ERR), is conducted on this central one-fiber unit cell, both in the
 case of an undamaged and of a partially debonded fiber.

Nomenclature and main features of the RVEs studied are described in the fol-
 lowing.

90 **$n \times k$ – free, Figure ??:** UD composite with thickness $t_{UD} = k \cdot 2L$, where
 k is the number of fiber “rows” in the vertical (through-the-thickness)
 direction and $2L$ the side length of the one-fiber unit cell as defined in
 Equation 1. Debonds appear only in the central fiber “row” with $n - 1$
 fully bonded fibers in between, where n is the number of fibers present in
 95 the RUC along the horizontal direction.

$n \times k$ – coupling, Figure ??: UD composite with multiple fiber “rows” con-

100 taining debonds with $n - 1$ fully bonded fibers in between, where n is the number of fibers present in the RUC along the horizontal direction. Fiber “rows” containing debonds are separated along the vertical (through-the-thickness) direction by $k - 1$ “rows” of fully bonded fibers, where k is the number of fiber “rows” present in the RUC along the vertical direction. Debonds that are vertically aligned are placed on the same side of their respective fiber. To model this configuration, conditions of coupling of the vertical displacement are applied on the top side.

105 **$n \times k$ – asymm, Figure ??:** same as in $n \times k$ – coupling, but debonds that are vertically aligned are placed on opposite sides of their respective fiber. To model this configuration, the following set of conditions is applied to the upper boundary:

$$\begin{aligned} u_z(x, kL) - u_z(0, kL) &= -(u_z(-x, kL) - u_z(0, kL)) \\ u_x(x, kL) &= -u_x(-x, kL) \end{aligned} \quad (2)$$

which represent conditions of anti-symmetric coupling [?].

110 **$n \times k - m \times t_{90^\circ}$, Figure ??:** Cross-ply laminate with 90° layer thickness $t_{90^\circ} = k \cdot 2L$ and 0° layer thickness $t_{0^\circ} = m \cdot t_{90^\circ}$. k is the number of fiber “rows” in the vertical (through-the-thickness) direction of the 90° layer and $2L$ the side length of the one-fiber unit cell as defined in Equation 1. Debonds are present only in the central fiber “row” of the 90° layer with $n - 1$ fully bonded fibers in between, where n is the number of fibers present in the RUC along the horizontal direction.

120 Every RUC is symmetric with respect to the horizontal (x) direction, thus only half of it is modeled in the FE solution through the use of symmetry boundary conditions on the bottom side. Conditions of coupling of the horizontal displacement are applied on the left and right side, to model the repetition of the RUC along the horizontal direction. A tensile load is applied on the right and left side in the form of displacement $\bar{u}_x = \pm \bar{\varepsilon}_x nL$ with $\bar{\varepsilon}_x = 1\%$. The

debond has a size of $2\Delta\theta$ (see Figure 1), with $\Delta\theta \geq 0$ ($\Delta\theta = 0$ is the case of no damage at all). For large debonds ($\Delta\theta \geq 60^\circ - 80^\circ$), a region called *contact zone*, of size $\Delta\Phi$ to be determined by the solution itself, appears at the crack tip. Correct resolution of this behavior requires the imposition of conditions of non-interpenetration of the crack faces. Crack face contact is assumed to be frictionless.

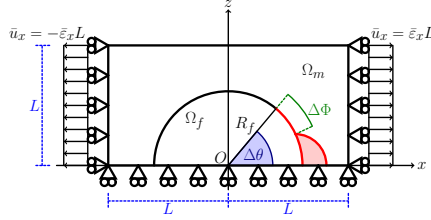


Figure 1: One-fiber unit cell and main parameters characterizing the debonding process.

The FE solution is obtained using Abaqus [?] using second order, 2D, plane strain triangular (CPE6) and rectangular (CPE8) elements. To accurately resolve the singularity at the crack tip, a regular mesh of only rectangular elements is used with almost unitary aspect ratio and angular size $\delta = 0.05^\circ$. The crack faces are represented as element-based surfaces with frictionless small-sliding contact pair interaction.

3. Dimensional analysis

We first recall that the Energy Release Rate G has units of energy E per unit area:

$$[G] = \frac{E}{L^2}, \quad (3)$$

where L stands for unit of length. By algebraic manipulation of Equation 3 we can write the units of ERR as

$$\frac{E}{L^2} = \frac{F \cdot L}{L^2} = \frac{F}{L^2} L, \quad (4)$$

140

where F stands for unit of force. We recognize that, in Equation 4

$$\frac{F}{L^2} = [\sigma] \quad \frac{L}{L} = [\varepsilon], \quad (5)$$

where σ and ε are respectively stress and strain. The reference Energy Release Rate is thus dimensionally equivalent to a reference stress σ_{ref} times a reference strain ε_{ref} times a reference length l_{ref} and we can write

$$G_0 \sim \sigma_{ref} \varepsilon_{ref} l_{ref}. \quad (6)$$

4. Linear Elastic Fracture Mechanics (LEFM) considerations

145

In the case of uniaxial loading, we can assume that: in a stress-controlled experiment, σ_{ref} is equal to the applied stress σ_0 and ε_{ref} to the average strain ε_0 in the Representative Volume Element (RVE); in a strain-controlled experiment, ε_{ref} is equal to the applied strain ε_0 and σ_{ref} to the average stress σ_{av} in the Representative Volume Element (RVE).

150

Under the assumption of linear elastic material constituents, we have, respectively for a stress- and strain-controlled experiment:

$$\varepsilon_{av} = E_{homo} \sigma_0 \quad \sigma_{av} = E_{homo} \varepsilon_0, \quad (7)$$

155

where E_{homo} is a homogenized RVE Young's modulus which measures the RVE elastic response in the presence of different material phases and damage. It is worth to point out here that, as we are interested in studying debond growth in the context of transverse crack onset, RVEs are loaded in the direction transverse to the fibers in the layer where debonds are present. Furthermore, we consider RVEs that are 2-dimensional and under the assumption of plane strain or plane stress conditions. This implies, considering the elastic response of a transversely isotropic material in its plane of transverse isotropy (indices 2 – 3, index 1 corresponds to the axis of rotational symmetry) with no damage, that [20, 21]

160

$$E_{homo} = \frac{E_2}{1 - \nu_{12}\nu_{21}} \quad E_{homo} = E_2, \quad (8)$$

respectively for plane strain and plane stress, with E_2 the homogenized transverse Young's modulus of the ply and ν_{12} , ν_{21} the major and minor Poisson's ratios. Notice that homogenized elastic properties depend on constituents' elastic properties and theIn the presence of damage, we can assume the homogenized Young's modulus of the damaged RVE to be a fraction of the undamaged modulus E_{homo}^0 (expressed in Eq. 8):

$$E_{homo} = f(\Delta\theta) E_{homo}^0, \quad (9)$$

where $0 < f(\Delta\theta) < 1$ is a function of the damage state in the material, in this case represented by the debond half-size $\Delta\theta$ (debond size is $2\Delta\theta$). By substituting Eq. 7, Eq. 8 and Eq. 9 in Eq. 6, we have

$$G_0 \sim f(\Delta\theta) \frac{E_2}{1 - \nu_{12}\nu_{21}} \varepsilon_0^2 l_{ref} \quad G_0 \sim f(\Delta\theta) E_2 \varepsilon_0^2 l_{ref}, \quad (10)$$

respectively for plane strain and plane stress conditions under applied strain ε_0 , and

$$G_0 \sim f(\Delta\theta) \frac{1 - \nu_{12}\nu_{21}}{E_2} \sigma_0^2 l_{ref} \quad G_0 \sim f(\Delta\theta) \frac{\sigma_0^2}{E_2} l_{ref}, \quad (11)$$

respectively for plane strain and plane stress conditions under applied strain σ_0 . Notice that, incidentally: the plane strain expression in Eq. 11 is the same as the ERR expression used for *in-situ* strenght modeling in [22] and derived in [23] by considering the fiber-reinforced polymer as a 3-phase composite with one phase constituted by sharp voids (cracks)¹; the plane stress expression in Eq. 11 is the same as the Mode I ERR in [24], derived from the definition of ERR and problem geometry.

¹Often expressed as $\Lambda_{22}^0 = 2 \left(\frac{1}{E_2} - \frac{\nu_{12}^2}{E_1} \right)$, which can be shown to be equivalent to $\Lambda_{22}^0 = 2 \frac{1 - \nu_{12}\nu_{21}}{E_2}$ by recalling that $\nu_{21} = \frac{E_2}{E_1} \nu_{12}$.

180 In accord with the classic Linear Elastic Fracture Mechanics (LEFM), the Energy Release Rate is directly proportional to the crack size a [25]. Given that $a = R_f 2\Delta\theta$ for debonds, where R_f is the fiber radius, it is reasonable to assume R_f as the reference length:

$$l_{ref} = R_f. \quad (12)$$

The reference Energy Release Rate thus becomes

$$G_0 \sim f(\Delta\theta) \frac{E_2}{1 - \nu_{12}\nu_{21}} \varepsilon_0^2 R_f \quad G_0 \sim f(\Delta\theta) E_2 \varepsilon_0^2 R_f, \quad (13)$$

185 respectively for plane strain and plane stress conditions under applied strain ε_0 , and

$$G_0 \sim f(\Delta\theta) \frac{1 - \nu_{12}\nu_{21}}{E_2} \sigma_0^2 R_f \quad G_0 \sim f(\Delta\theta) \frac{\sigma_0^2}{E_2} R_f, \quad (14)$$

respectively for plane strain and plane stress conditions under applied strain σ_0 .

5. Similarity and geometry correction factor

190 In agreement with the classic Fracture Mechanics (FM) treatment [25], we can recognize in the function $f(\Delta\theta)$ of Eq. 13 and Eq. 14 the geometry correction factor ($f(a)$ or Y) that establishes the relation of similarity [26]

$$K = f(a) \sigma \sqrt{a} \quad \text{or} \quad G = f^2(a) \frac{\sigma^2}{E} a \quad (15)$$

between the Stress Intensity Factor (SIF) K and Energy Release Rate (ERR) G of a generic configuration of structural and crack geometry and the solution
195 for a Center Crack (CC) in an infinite plate

$$K_{CC} = \sigma \sqrt{a} \quad \text{or} \quad G_{CC} = \frac{\sigma^2}{E} a, \quad (16)$$

where the crack size is $2a$. It thus seems reasonable to look for a functional form of $f(\Delta\theta)$ in Eq. 13 and Eq. 14 among known analytical solutions of SIFs

and ERRs and such that a physically-meaningful similarity between the two configurations could be established.

- 200 • **Straight central crack in an infinite isotropic plate under far-field transverse tension [25].**

$$f_I(\Delta\theta) = \sin(\Delta\theta) \quad f_{II}(\Delta\theta) = 0 \quad (17)$$

It is the simplest choice, based on considering the debond chord $2R_f \sin \Delta\theta$ as its representative size. However, as apparent in Eq. 17, there is no Mode II geometry correction factor available (a straight crack in transverse tension propagates only in Mode I) and it is thus not suited to establish a relation of similarity with debond ERR, which is Mode II dominated for large $\Delta\theta$.

- 205 • **Inclined central crack in an infinite isotropic plate under far-field tension [25].**

$$\begin{aligned} f_I(\Delta\theta) &= \sin(\Delta\theta) \sin^4\left(\frac{\pi}{2} - \Delta\theta\right) \\ f_{II}(\Delta\theta) &= \sin(\Delta\theta) \sin^2\left(\frac{\pi}{2} - \Delta\theta\right) \cos^2\left(\frac{\pi}{2} - \Delta\theta\right) \end{aligned} \quad (18)$$

210 A first attempt to amend the shortcomings of Eq. 17 is to consider the geometry correction factor of the inclined crack subjected to transverse load. However, $f_{II}(90^\circ) = 0$ in Eq. 18, which makes also this choice not a good choice to establish a similarity relation with debond ERR (Mode II ERR is well-defined and different from 0 at $\Delta\theta = 90^\circ$ for debonds).

- 215 • **Circular crack in an infinite isotropic plate under far-field tension transverse to crack's chord [27].**

$$\begin{aligned}
f_I(\Delta\theta) &= \frac{G_I}{\sigma_{ref}\varepsilon_{ref}R} = \frac{1}{2} \sin(\Delta\theta) \times \\
&\times \left(\frac{1 - \sin^2\left(\frac{\Delta\theta}{2}\right) \cos^2\left(\frac{\Delta\theta}{2}\right)}{1 + \sin^2\left(\frac{\Delta\theta}{2}\right)} \cos\left(\frac{\Delta\theta}{2}\right) + \cos\left(\frac{3}{2}\Delta\theta\right) \right)^2 \\
f_{II}(\Delta\theta) &= \frac{G_{II}}{\sigma_{ref}\varepsilon_{ref}R} = \frac{1}{2} \sin(\Delta\theta) \times \\
&\times \left(\frac{1 - \sin^2\left(\frac{\Delta\theta}{2}\right) \cos^2\left(\frac{\Delta\theta}{2}\right)}{1 + \sin^2\left(\frac{\Delta\theta}{2}\right)} \sin\left(\frac{\Delta\theta}{2}\right) + \sin\left(\frac{3}{2}\Delta\theta\right) \right)^2
\end{aligned} \tag{19}$$

The geometry correction factors of Eq. 19 (shown in Fig. 2) present a solution to the issues characterising Eq. 17 and Eq. 18: Mode II is defined and both modes are defined and continuous for $\Delta\theta = 0^\circ - 180^\circ$. By evaluating the elastic properties E_2 , ν_{12} and ν_{21} at the value of V_f of the composite under consideration and substituting Eq. 19 in Eq. 14 and Eq. 13, we obtain the Mode I G_{I0} and Mode II G_{II0} ERR of a circular crack of size $a = 2\Delta\theta$ in an infinite isotropic medium, which has properties equivalent to the elastic properties of a UD composite of fiber volume fraction V_f in its plane of transverse isotropy, obtained by application of the Concentric Cylinders Assembly [28] with Self-Consistent Shear [29] (CCA-SCS) model. The following expressions are derived,

1. under plane strain conditions and applied far-field transverse strain:

$$\begin{aligned}
G_{I0} &= f_I(\Delta\theta) \frac{E_2(V_f)}{1 - \nu_{12}(V_f)\nu_{21}(V_f)} \varepsilon_0^2 R_f \\
G_{II0} &= f_{II}(\Delta\theta) \frac{E_2}{1 - \nu_{12}\nu_{21}} \varepsilon_0^2 R_f;
\end{aligned} \tag{20}$$

2. under plane strain conditions and applied far-field transverse stress:

$$\begin{aligned}
G_{I0} &= f_I(\Delta\theta) \frac{1 - \nu_{12}(V_f)\nu_{21}(V_f)}{E_2(V_f)} \sigma_0^2 R_f \\
G_{II0} &= f_{II}(\Delta\theta) \frac{1 - \nu_{12}(V_f)\nu_{21}(V_f)}{E_2(V_f)} \sigma_0^2 R_f
\end{aligned} \tag{21}$$

3. under plane stress conditions and applied far-field transverse strain:

$$\begin{aligned}
G_{I0} &= f_I (\Delta\theta) E_2 (V_f) \varepsilon_0^2 R_f \\
G_{II0} &= f_{II} (\Delta\theta) E_2 (V_f) \varepsilon_0^2 R_f
\end{aligned} \tag{22}$$

4. under plane stress conditions and applied far-field transverse stress:

$$\begin{aligned}
G_{I0} &= f_I (\Delta\theta) \frac{\sigma_0^2}{E_2 (V_f)} R_f \\
G_{II0} &= f_{II} (\Delta\theta) \frac{\sigma_0^2}{E_2 (V_f)} R_f
\end{aligned} \tag{23}$$

This configuration thus establishes a physically-meaningful relation of similarity, as the ratios $\frac{G_I}{G_{I0}} = g_I (\Delta\theta, V_f) [-]$ and $\frac{G_{II}}{G_{II0}} = g_{II} (\Delta\theta, V_f) [-]$ measure the effect of: the mismatch in elastic properties between phases (in Eq. 19 the medium is isotropic); the finite size of the geometry (in Eq. 19 the medium is infinite); the interaction with neighboring undamaged and partially debonded fibers, a free surface (in UD composites) or the $0^\circ/90^\circ$ interface (in cross-ply laminates).

Given that debond ERR for RVEs presented in Section ?? is evaluated under conditions of plane strain and applied transverse strain, the expressions of G_{I0} and G_{II0} in Eq. 20 are adopted in the following.

6. Effect of elastic properties mismatch

7. Effect of fiber volume fraction

8. Effect of neighboring fibers

References

- [1] A. Kopp, S. Stappert, D. Mattsson, K. Olofsson, E. Marklund, G. Kurth, E. Mooij, E. Roorda, The aurora space launcher concept, CEAS Space Journal 10 (2) (2017) 167–187. doi:10.1007/s12567-017-0184-2.

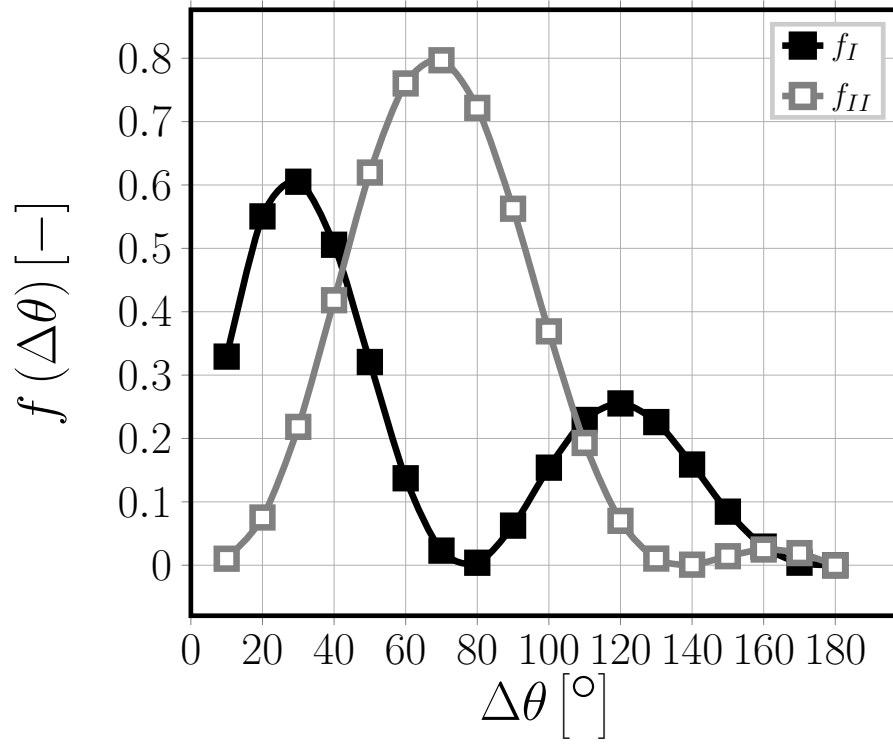


Figure 2: Mode I (f_I) and Mode II (f_{II}) geometry correction functions for a circular crack in infinite isotropic medium. The chord of the crack is normal to the loading direction and the crack size is $a = 2\Delta\theta$.

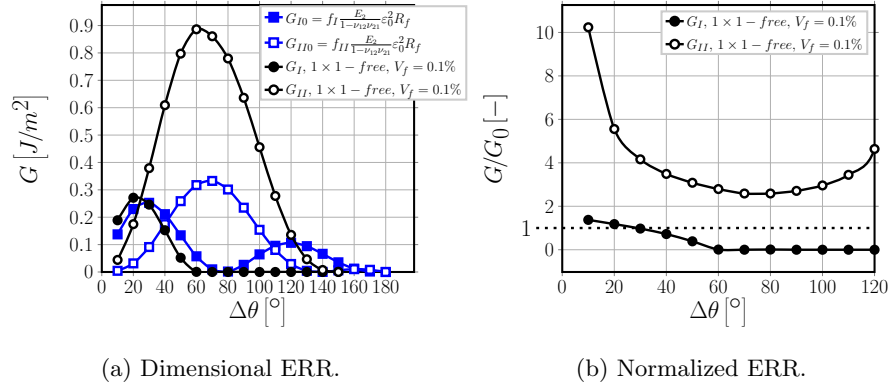


Figure 3: *Left*: Mode I and Mode II ERR for the circular crack in an infinite isotropic medium (G_{I0} and G_{II0}) and for a single partially debonded fiber in an infinite matrix ($1 \times 1 - free$, $V_f = 0.1\%$). In G_{I0} and G_{II0} , E_2 , ν_{12} and ν_{21} are evaluated using the Concentric Cylinders Assembly [28] with Self-Consistent Shear [29] (CCA-SCS) model for $V_f = 0.1\%$. In both cases, a transverse load is applied in the form of transverse strain ε_x of 1%. *Right*: Mode I and Mode II ERR of single partially debonded fiber in an infinite matrix ($1 \times 1 - free$, $V_f = 0.1\%$) normalized by Mode I and Mode II ERR of the circular crack in an infinite isotropic medium (G_{I0} and G_{II0}).

- [2] J. Cugnoni, R. Amacher, S. Kohler, J. Brunner, E. Kramer, C. Dransfeld, W. Smith, K. Scobbie, L. Sorensen, J. Botsis, Towards aerospace grade thin-ply composites: Effect of ply thickness, fibre, matrix and interlayer toughening on strength and damage tolerance, Composites Science and Technology 168 (2018) 467–477. doi:10.1016/j.compscitech.2018.08.037.
- [3] H. Sasayama, K. Kawabe, S. Tomoda, I. Ohsawa, K. Kageyama, N. Ogata, Effect of lamina thickness on first ply failure in multidirectionally laminated composites, in: Proceedings of the 8th Japan SAMPE Symposium, SAMPE, 2003.
- [4] H. Saito, H. Takeuchi, I. Kimpara, Experimental evaluation of the damage growth restraining in 90 layer of thin-ply cfrp cross-ply laminates, Advanced Composite Materials 21 (1) (2012) 57–66. doi:10.1163/156855112X629522.

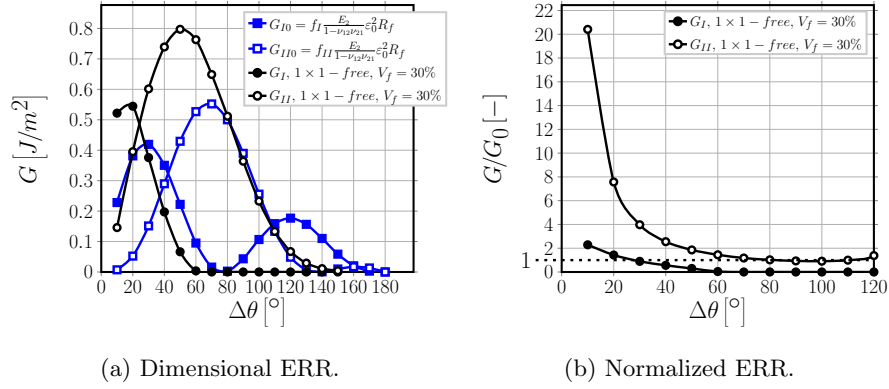


Figure 4: *Left*: Mode I and Mode II ERR for the circular crack in an infinite isotropic medium (G_{I0} and G_{II0}) and for a single partially debonded fiber in an infinite matrix ($1 \times 1 - free$, $V_f = 30\%$). In G_{I0} and G_{II0} , E_2 , ν_{12} and ν_{21} are evaluated using the Concentric Cylinders Assembly [28] with Self-Consistent Shear [29] (CCA-SCS) model for $V_f = 30\%$. In both cases, a transverse load is applied in the form of transverse strain ε_x of 1%. *Right*: Mode I and Mode II ERR of single partially debonded fiber in an infinite matrix ($1 \times 1 - free$, $V_f = 30\%$) normalized by Mode I and Mode II ERR of the circular crack in an infinite isotropic medium (G_{I0} and G_{II0}).

- [5] R. Amacher, J. Cugnoni, J. Botsis, L. Sorensen, W. Smith, C. Dransfeld, Thin ply composites: Experimental characterization and modeling of size-effects, Composites Science and Technology 101 (2014) 121–132. doi:10.1016/j.compscitech.2014.06.027.
- [6] J. E. Bailey, P. T. Curtis, A. Parvizi, On the transverse cracking and longitudinal splitting behaviour of glass and carbon fibre reinforced epoxy cross ply laminates and the effect of poisson and thermally generated strain, Proceedings of the Royal Society A: Mathematical, Physical and Engineering Sciences 366 (1727) (1979) 599–623. doi:10.1098/rspa.1979.0071.
- [7] J. E. Bailey, A. Parvizi, On fibre debonding effects and the mechanism of transverse-ply failure in cross-ply laminates of glass fibre/thermoset composites, Journal of Materials Science 16 (3) (1981) 649–659. doi:10.1007/bf02402782.

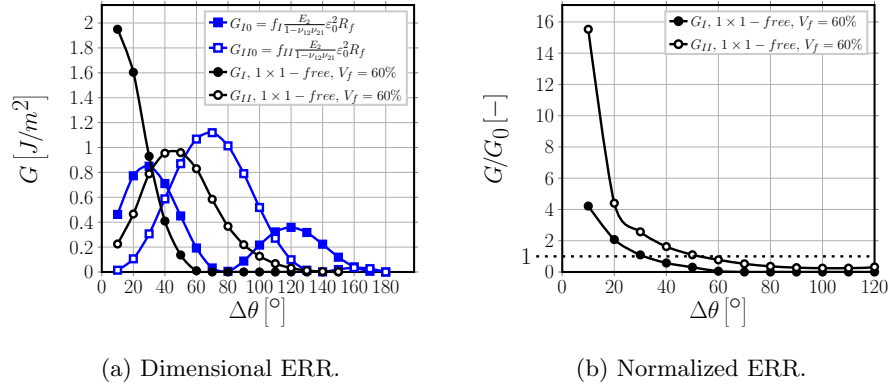


Figure 5: *Left*: Mode I and Mode II ERR for the circular crack in an infinite isotropic medium (G_{I0} and G_{II0}) and for a single partially debonded fiber in an infinite matrix ($1 \times 1 - free$, $V_f = 60\%$). In G_{I0} and G_{II0} , E_2 , ν_{12} and ν_{21} are evaluated using the Concentric Cylinders Assembly [28] with Self-Consistent Shear [29] (CCA-SCS) model for $V_f = 60\%$. In both cases, a transverse load is applied in the form of transverse strain ε_x of 1%. *Right*: Mode I and Mode II ERR of single partially debonded fiber in an infinite matrix ($1 \times 1 - free$, $V_f = 60\%$) normalized by Mode I and Mode II ERR of the circular crack in an infinite isotropic medium (G_{I0} and G_{II0}).

[8] L. Asp, L. Berglund, R. Talreja, Prediction of matrix-initiated transverse failure in polymer composites, *Composites Science and Technology* 56 (9) (1996) 1089–1097. doi:10.1016/0266-3538(96)00074-7.

[9] J. A. Kies, Maximum strains in the resin of fibreglass composites, Nrl report 5752, ad-274560, Washington (DC): U.S. Naval Research Laboratory (1962).

[10] H. Zhang, M. Ericson, J. Varna, L. Berglund, Transverse single-fibre test for interfacial debonding in composites: 1. experimental observations, *Composites Part A: Applied Science and Manufacturing* 28 (4) (1997) 309–315. doi:10.1016/s1359-835x(96)00123-6.

[11] F. París, E. Correa, V. Mantić, Kinking of transversal interface cracks between fiber and matrix, *Journal of Applied Mechanics* 74 (4) (2007) 703. doi:10.1115/1.2711220.

- [12] L. Zhuang, R. Talreja, J. Varna, Transverse crack formation in unidirectional composites by linking of fibre/matrix debond cracks, *Composites Part A: Applied Science and Manufacturing* 107 (2018) 294–303. doi:10.1016/j.compositesa.2018.01.013.
- [13] L. Zhuang, A. Pupurs, J. Varna, R. Talreja, Z. Ayadi, Effects of inter-fiber spacing on fiber-matrix debond crack growth in unidirectional composites under transverse loading, *Composites Part A: Applied Science and Manufacturing* 109 (2018) 463–471. doi:10.1016/j.compositesa.2018.03.031.
- [14] C. Sandino, E. Correa, F. París, Numerical analysis of the influence of a nearby fibre on the interface crack growth in composites under transverse tensile load, *Engineering Fracture Mechanics* 168 (2016) 58–75. doi:10.1016/j.engfracmech.2016.01.022.
- [15] J. Varna, L. Q. Zhuang, A. Pupurs, Z. Ayadi, Growth and interaction of debonds in local clusters of fibers in unidirectional composites during transverse loading, *Key Engineering Materials* 754 (2017) 63–66. doi:10.4028/www.scientific.net/kem.754.63.
- [16] C. Sandino, E. Correa, F. París, Interface crack growth under transverse compression: nearby fibre effect, in: *Proceeding of the 18th European Conference on Composite Materials (ECCM-18)*, 2018.
- [17] M. Comninou, The interface crack, *Journal of Applied Mechanics* 44 (4) (1977) 631. doi:10.1115/1.3424148.
- [18] M. Toya, A crack along the interface of a circular inclusion embedded in an infinite solid, *Journal of the Mechanics and Physics of Solids* 22 (5) (1974) 325–348. doi:10.1016/0022-5096(74)90002-7.
- [19] F. París, J. C. Caño, J. Varna, The fiber-matrix interface crack — a numerical analysis using boundary elements, *International Journal of Fracture* 82 (1) (1996) 11–29. doi:10.1007/bf00017861.

- [20] S. P. Timoshenko, J. N. Goodier, Theory of elasticity, Engineering societies monographs, McGraw-Hill, 1987.
- [21] V. Mantič, Interface crack onset at a circular cylindrical inclusion under
 320 a remote transverse tension. application of a coupled stress and energy
 criterion, International Journal of Solids and Structures 46 (6) (2009) 1287–
 1304. doi:10.1016/j.ijsolstr.2008.10.036.
- [22] P. P. Camanho, C. G. Dvila, S. T. Pinho, L. Iannucci, P. Robinson,
 325 Prediction of in situ strengths and matrix cracking in composites un-
 der transverse tension and in-plane shear, Composites Part A: Applied
 Science and Manufacturing 37 (2) (2006) 165 – 176, compTest 2004.
 doi:10.1016/j.compositesa.2005.04.023.
- [23] N. Laws, G. Dvorak, M. Hejazi, Stiffness changes in unidirectional com-
 posites caused by crack systems, Mechanics of Materials 2 (2) (1983) 123
 330 – 137. doi:10.1016/0167-6636(83)90032-7.
- [24] J. Varna, 2.10 crack separation based models for microcracking, in:
 P. W. Beaumont, C. H. Zweben (Eds.), Comprehensive Composite
 Materials II, Elsevier, Oxford, 2018, pp. 192 – 220. doi:10.1016/
 B978-0-12-803581-8.09910-0.
- [25] H. Tada, P. Paris, G. Irwin, The Stress Analysis of Cracks Handbook,
 335 ASME Press, 2000.
- [26] G. I. Barenblatt, Scaling phenomena in fatigue and fracture, Inter-
 national Journal of Fracture 138 (1-4) (2006) 19–35. doi:10.1007/
 s10704-006-0036-0.
- [27] N. I. Ioakmidis, P. S. Theocaris, Array of periodic curvilinear cracks in an
 340 infinite isotropic medium, Acta Mechanica 28 (1) (1977) 239–254. doi:
 10.1007/BF01208801.
- [28] Z. Hashin, Analysis of composite materials—a survey, Journal of Applied
 Mechanics 50 (3) (1983) 481. doi:10.1115/1.3167081.

- ³⁴⁵ [29] R. Christensen, K. Lo, Solutions for effective shear properties in three phase sphere and cylinder models, *Journal of the Mechanics and Physics of Solids* 27 (4) (1979) 315–330. doi:10.1016/0022-5096(79)90032-2.

9. Conclusions